CMS Physics Analysis Summary

Contact: cms-pag-conveners-susy@cern.ch 2011/07/23

Search for new physics with same-sign isolated dilepton events with jets and missing energy

The CMS Collaboration

Abstract

The results of a search for new physics in events with two same-sign isolated leptons (electrons, muons, or hadronically decaying tau-leptons), hadronic jets, and missing transverse energy in the final state are presented. These results are based on analysis of a data sample with a corresponding integrated luminosity of 0.98 fb^{-1} produced in pp collisions at a center-of-mass energy of 7 TeV collected by the CMS experiment at the LHC. The observed numbers of events agree with the standard model predictions, and no evidence for new physics is found. These observations are used to set upper limits on the number of events from new physics contributions and to constrain supersymmetric models.

1 Introduction

Events with same-sign isolated lepton pairs from hadron collisions are very rare in the standard model (SM) but appear very naturally in many new physics scenarios. In particular, they have been proposed as signatures of supersymmetry (SUSY) [1–3], universal extra dimensions [4], pair production of $T_{5/3}$ (a fermionic partner of the top quark) [5], heavy Majorana neutrinos [6], and same-sign top-pair resonances as predicted in theories with warped extra dimensions [7].

In this summary we describe searches for new physics with same-sign isolated dileptons (ee, eμ, $\mu\mu$, eτ, $\mu\tau$, and $\tau\tau$, where taus decay hadronically, and electron or muon final states naturally include leptonic tau decays), missing transverse energy ($E_{\mathrm{T}}^{\mathrm{miss}}$), and hadronic jets. Our choice of signal regions is driven by two simple observations. First, astrophysical evidence for dark matter [8] suggests that we concentrate on final states with $E_{\mathrm{T}}^{\mathrm{miss}}$. Second, observable new physics signals with large cross sections are likely to be produced by strong interactions, and we thus expect significant hadronic activity in conjunction with the two same-sign leptons. Beyond these simple guiding principles, our searches are as independent of detailed features of new physics models as possible. The results are based on a data sample corresponding to an integrated luminosity of 0.98 fb^{-1} collected in pp collisions at a center-of-mass energy of 7 TeV by the Compact Muon Solenoid (CMS) experiment at the Large Hadron Collider (LHC) in 2011. This analysis constitutes an update to the previous CMS results based on the 2010 data [9] and expands the sensitivity to new physics models by increasing the data sample and adding new signal selections.

This summary is organized as follows. The CMS detector is briefly described in Section 2. The reconstruction of leptons, $E_{\mathrm{T}}^{\mathrm{miss}}$, and jets in CMS is summarized in Section 3, followed by a description of the baseline selections in Section 4. Section 5 describes our search regions. The dominant backgrounds are estimated from data, as discussed in Section 6. Systematic uncertainties on the predicted number of signal events and results are discussed in Sections 7 and 8. We conclude with a discussion on how to use our results to constrain a wide variety of new physics models in Section 9.

2 The CMS Detector

A right-handed coordinate system is employed by the CMS experiment, with the origin at the nominal interaction point, the x-axis pointing to the center of the LHC, and the y-axis pointing up (perpendicular to the LHC plane). The polar angle θ is measured from the positive z-axis and the azimuthal angle ϕ is measured in the xy plane. The pseudorapidity is defined as $\eta = -\ln[\tan(\frac{\theta}{2})]$. The CMS detector is a general purpose hadron collider detector. It is a nearly hermetic detector with calorimetry (electromagnetic (ECAL) and hadron (HCAL)) extending to $|\eta| < 5$ and a charged particle magnetic spectrometer with a coverage within $|\eta| < 2.5$, including a muon detector extending to $|\eta| < 2.4$. A two-tier trigger system is designed to select the most interesting pp collision events for use in physics analysis. A detailed description of the CMS detector can be found elsewhere [10].

3 Reconstruction of Leptons, Missing Energy, and Jets

Muons, electrons, and hadronically decaying taus are included in the analysis. All lepton candidates are required to have $|\eta| < 2.4$, and be consistent with originating from the same interaction vertex. The selection efficiencies for electrons and muons are measured in data and simulation using events with leptonically decaying Z bosons. The difference in results ob-

tained in data and simulation is used to correct the simulated yields in simulated signal events. A standard tag-and-probe method [11] is employed for electrons and muons. The efficiencies for taus are estimated in simulation, comparisons with values measured in data can be found in Ref. [12].

Muon candidates are required to be successfully reconstructed [13] using two algorithms, one in which tracks in the silicon detector are matched to consistent signals in the calorimeters and muon system, and another in which a simultaneous global fit is performed to hits in the silicon tracker and muon system. The track associated with the muon candidate is required to have a minimum number of hits in the silicon tracker, have a high-quality global fit including a minimum number of hits in the muon detectors, and have calorimeter energy deposits consistent with originating from a minimum ionizing particle. The identification efficiency measured in data is approximately 96% for muons of all momenta.

Electron candidates are reconstructed [14] starting from a cluster of energy deposits in the ECAL, which is then matched to hits in the silicon tracker. A selection using electron identification variables based on shower shape and track-cluster matching is applied to the reconstructed candidates; the criteria are optimized in the context of the inclusive $W \to e\nu$ measurement [11] and are designed to maximally reject electron candidates from QCD multijet production while maintaining approximately 80% efficiency for electrons from the decay of W/Z bosons. Electron candidates within $\Delta R \equiv \sqrt{\Delta\phi^2 + \Delta\eta^2} < 0.1$ of a muon are rejected to remove electron candidates due to muon bremsstrahlung and final-state radiation. Electron candidates originating from photon conversions are suppressed by looking for a partner track and requiring no missing hits for the track fit in the inner layers of the tracking detectors. The electron identification efficiency varies from 43% in the range of p_{T} of 10-15 GeV/c to 84% for electrons with $p_{\mathrm{T}} > 40$ GeV/c.

Hadronic τ candidates (later referred to simply as τ) are identified [15] starting with a hadronic jet clustered from the particles reconstructed using the particle-flow global-event reconstruction algorithm [16]. The pion with the highest transverse momentum (p_T) that resides within a cone of $\Delta R < 0.1$ around the jet axis is required to be greater than 5 GeV. A variable size cone of $\Delta R < 5$ GeV$/p_T$ is then defined around the leading track, and the boosted τ-decay products are expected to be confined within this narrow cone. Only τ candidates with one or three charged hadrons in this cone are selected. The charged hadrons are then combined with the reconstructed neutral pions to identify the hadronic tau decay mode. The reconstructed tau candidates having at least one charged hadron or photon ($p_T > 0.8$ GeV) not associated to the tau decay signature within an isolation cone of $\Delta R < 0.5$ are rejected. The τ selection efficiency is estimated directly in simulation, no direct comparison is done with available measurements in Z-boson events. For the reference signal LM6 benchmark point, defined in Section 5, it varies from almost zero at 15 GeV to 25% at 40 GeV, reaching the maximum at 34% for momenta above 80 GeV.

Charged leptons from the decay of W/Z bosons, as well as the new physics we are searching for, are expected to be isolated from other activity in the event. We calculate a relative measure of this isolation denoted as I_{rel}. This quantity is defined as the ratio of the scalar sum of transverse track momenta and transverse calorimeter energy deposits within a cone of $\Delta R < 0.3$ around the lepton candidate direction at the origin, to the transverse momentum of the candidate. The contribution from the candidate itself is excluded. Electrons and muons with $I_{\mathrm{rel}} < 0.15$ are considered isolated. The isolation efficiency for Z-boson events changes from approximately 60% for muons in the 5–10 GeV/c range, 77% (87%) for muons (electrons) in 10–15 GeV/c range, and has a value above 99% for $p_{\mathrm{T}} > 40$ GeV.

In order to suppress the background due to dileptons originating from the same jet, we require that selected dileptons have a minimum invariant mass of 5 GeV. This helps to keep dileptons uncorrelated with respect to their I_{rel} observables, which is a feature we exploit in the analysis. We also remove events with a third lepton of opposite sign and same flavor as one of the two selected leptons if the invariant mass of the pair is between 76 and 106 GeV. This requirement further reduces an already small background contribution from WZ and ZZ production.

Jets and $E_{\text{T}}^{\text{miss}}$ are reconstructed based on the particle-flow technique [16, 17]. For jet clustering, we use the anti-k_T algorithm with the distance parameter $R = 0.5$ [18]. Jets are required to pass standard quality requirements [19] to remove those consistent with calorimeter noise. After the expected contribution from extra pp collisions is subtracted, jet energies are corrected for residual non-uniformity and nonlinearity of the detector response derived using collision data [20]. We require jets to have $p_{\text{T}} > 40$ GeV and $|\eta| < 2.5$ to be considered for analysis. We define the H_{T} observable as the scalar sum of the p_T of all such jets with $\Delta R > 0.4$ to the nearest lepton passing all our requirements.

4 Baseline Selections

Muon, electron, and tau candidates with p_T as low as 5, 10, and 15 GeV respectively, and with $|\eta| < 2.4$, are used to define the dilepton final states. All events considered for search regions are required to have two leptons with the same charge, at least two jets, and $E_{\text{T}}^{\text{miss}}$ above 30 GeV. The requirement of at least two jets provides a universal requirement of $H_{\text{T}} > 80$ GeV.

Leptons in processes beyond the SM can appear in decays of W or Z bosons as well as in sequential decays of new particles. A large part of the p_{T} spectrum in W or Z-boson decays is above 20 GeV, while in the sequential decays lepton momentum may be low. Less restrictive requirements on the lepton momentum implies higher rate of background events. This is balanced by an increasing requirement on H_{T} or $E_{\text{T}}^{\text{miss}}$.

We begin by defining the following three baseline selections:

- *inclusive dileptons*: events with $\mu\mu$, ee, or $e\mu$ dilepton candidates and $H_{\text{T}} > 200$ GeV;
- *high-p_{T} dileptons*: events with $\mu\mu$, ee, or $e\mu$ dilepton candidates with both leptons having $p_{\text{T}} > 10$ GeV, at least one lepton having $p_{\text{T}} > 20$ GeV, and no additional H_{T} requirement beyond $H_{\text{T}} > 80$ GeV arising from the requirement to have at least two jets;
- *τ dileptons*: events with $\tau\tau$, $e\tau$, or $\mu\tau$ dilepton candidates, $H_{\text{T}} > 350$ GeV, and $E_{\text{T}}^{\text{miss}} > 80$ GeV.

These baseline selections provide a reasonably large number of events in the data sample to be able to test the methods of background predictions.

Separate types of selection algorithms (triggers) are used to collect events in each of these baseline selections. The *inclusive dilepton* events are selected with triggers requiring both a dilepton and an H_T above 150 GeV to be present. The *high-p_{T} dilepton* events are collected with triggers demanding the presence of two leptons with higher transverse momenta and no requirement on H_{T}. Triggers for hadronic τ-leptons are intrinsically prone to high rates. Therefore, special triggers, which rely on significant H_T and $E_{\text{T}}^{\text{miss}}$, as well as the presence of a single lepton or two hadronic τ-leptons, are used for the *τ dilepton* selection. It is worth noting that the used triggers also provide several control samples, which are necessary for the evaluation of backgrounds. The requirements on lepton momenta, H_{T}, and $E_{\text{T}}^{\text{miss}}$ in the baseline selections are limited to the

regions above the thresholds applied in the triggers.

Selection of leptons by the triggers is the most efficient for electrons and the least efficient for hadronic taus, considering leptons passing identification and isolation requirements described above. For electrons the efficiency is in a range of 98–99%, as measured in Z events using the tag-and-probe method. The efficiency for muons changes from 90% at 5 GeV to 96% for momenta higher than 10 GeV. The efficiency for hadronic taus is approximately 90% [21]. Selection of $H_T > 150$ GeV by the trigger results in an efficiency of approximately 99% in the range of reconstructed H_T above 200 GeV. Triggers used for the selection of the τ-*dileptons* require a E_T^{miss} above 35 GeV for most of the data taking. The efficiency of this requirement for events passing the baseline selections is above 95%.

5 Search Regions

The three dilepton baseline regions cover the widest possible phase space. The motivation for covering the widest possible phase space in this search can be illustrated by an example of a SUSY cascade, shown in Fig. 1, naturally giving rise to jets, E_T^{miss}, and same-sign leptons: (gluinos/squarks) $\rightarrow$ (charged gaugino) $\rightarrow$ (lightest supersymmetric particle (LSP) neutralino). The mass difference between the gluino/squarks and the charged gaugino, typically arbitrary, defines the amount of hadronic activity one may expect in the event. The mass difference between the gaugino and a neutralino influences the lepton p_T spectrum. Depending on the nature of the chargino and neutralino, their mass difference can be either arbitrary (e.g., wino and bino) or typically small (e.g., higgsinos). Moreover, there is a range of scenarios where a large production asymmetry exists between τ and e/μ leptons. This motivates us to look specifically for events with a τ.

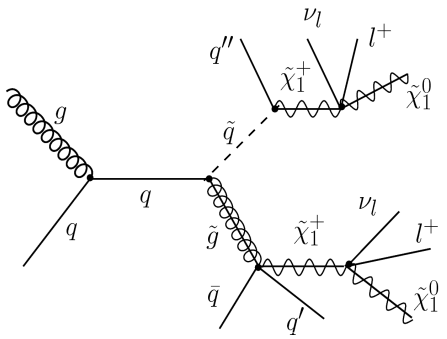

Figure 1: An example of a process involving the production and decays of SUSY particles, which gives rise to two same-sign prompt leptons, jets, and missing transverse energy.

Events passing the baseline selections provide a sample still expected to be dominated by backgrounds. Further selections are applied to restrict the baseline sample to the regions where the analysis is sensitive to potential new physics. As a reference model, we use LM6, a point in the constrained Minimal Supersymmetric Standard Model (CMSSM) [22] defined with the model parameters $m_0 = 85$ GeV, $m_{1/2} = 400$ GeV, $\tan\beta = 10$, $\mu > 0$, and $A_0 = 0$ GeV.

The following inclusive search regions are defined, constraining the baseline selection categories, starting from the most restrictive one:

1. *high-H_T high-E_T^{miss}* with $H_T > 400$ GeV and $E_T^{miss} > 120$ GeV, providing a high expected sensitivity to the CMSSM with low values of m_0, as in LM6;

2. *medium-H_T high-E_T^{miss}* with $H_T > 200$ GeV and $E_T^{miss} > 120$ GeV, targets models with moderate mass-splittings between $\tilde{g}/\tilde{q}$ and $\tilde{\chi}_1^+/\tilde{\chi}_2^0$;

3. *high-H_T low-E_T^{miss}* with $H_T > 400$ GeV and $E_T^{miss} > 50$ GeV, providing a high expected sensitivity to CMSSM with high values of m_0;

4. *low-H_T high-E_T^{miss}* with $H_T > 80$ GeV and $E_T^{miss} > 100$ GeV, providing a high expected sensitivity to models predicting low hadronic activity with a high E_T^{miss}, like those with sneutrino LSP in the context of phenomenological MSSM (pMSSM) [23, 24].

The thresholds on H_T and E_T^{miss} used to define the search regions are chosen not only to accommodate trigger thresholds and to probe distinct regions of the parameter space, but also to both limit and diversify our exposure to the standard model backgrounds. When comparing the search regions to the baseline selections, one will readily observe that search region 4 is only accessible to the *high-p_T dileptons*, and that the *τ-dileptons* component of this analysis can only probe search region 1.

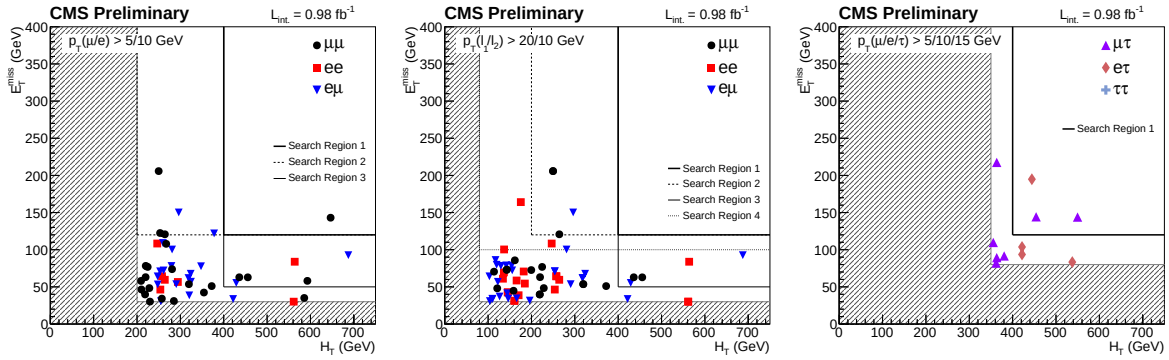

Figure 2: H_T versus E_T^{miss} scatter plots for the three baseline regions in data: *inclusive dileptons* (left), *high-p_T dileptons* (center), and *τ-dileptons* (right).

Figure 2 shows the events observed in data on the H_T–E_T^{miss} plane for the three baseline selection categories. The gray shaded area in each plot represents the phase space that is not considered for a baseline or a search region, as it is dominated by background and is typically outside of the trigger acceptance. The dashed and solid lines denote the boundaries of the respective search regions. Most of events observed in data have rather low values of H_T and E_T^{miss}, and do not fall into any of the search regions.

6 Background Estimation

Standard model sources of same-sign dilepton events with both leptons coming from a W or Z decay are very small in our data sample. Simulation-based predictions of the combined yields for $q\bar{q} \to WZ$ and ZZ, double "W-strahlung" $qq \to q'q'W^{\pm}W^{\pm}$, double parton scattering $2 \times (q\bar{q} \to W^{\pm})$, and $t\bar{t}W$ comprise a fraction of about 10% to 40% of the total background in the final states considered, the smallest in the baseline selections and the largest in search region 1 (high-H_T and high-E_T^{miss}). As these processes have never been measured in proton-proton collisions, apart from WZ [25], and their background contributions are very small, we evaluate them using simulation,[1] assigning a 50% systematic uncertainty. The background contribution

[1] We have ignored the triple-boson WWW or alike contributions.

from pp $\rightarrow$ Wγ, where the W decays leptonically and the photon converts in the detector material giving rise to an isolated electron, is also estimated from simulation and contributes less than 15% of simulated background events.

Backgrounds in all of our searches are dominated by one or two jets mimicking the lepton signature. Such lepton candidates can be genuine leptons from heavy-flavor decays, electrons from unidentified photon conversions, muons from meson decays in flight, hadrons reconstructed as leptons, or jet fluctuations leading to hadronic τ signatures. We will refer to all of these as "fake leptons". Leptons from decays of W, Z, gauginos, and other particles, which constitute the signal we are searching for, will be referred to as "prompt leptons". For the ee and eμ final states, electron charge misreconstruction due to hard bremsstrahlung poses another potentially important background, as there are significant opposite-sign ee and eμ contributions, especially from $\mathrm{t\bar{t}}$, where both W bosons from the top quarks decay leptonically.

Essentially, the same methods employed in Ref. [9] are used in searches described here. Highlights of the methods and significant changes are described below. Details of the definition and implementation of the methods can be found in the original reference.

6.1 Events with fake leptons

Contributions from events with fake electrons, muons, or taus include multijet processes where both leptons must be faked, and electroweak processes like W+jets, $\mathrm{t\bar{t}}$, and single-t where only one must be faked. The events with one fake lepton passing the baseline or tighter selections in simulation are expected to be predominantly from $\mathrm{t\bar{t}}$ events where the fake lepton arises from a heavy-flavor quark decay. Several methods applied earlier in Ref. [9] are used here to estimate the number of events with fake electrons or muons using control data samples. All are shown to give consistent estimates of this background. Contributions from fake electrons or muons in the τ-*dilepton* selections are negligible in comparison to those from τ. Thus the fake tau contribution is considered separately.

Leptons failing the nominal (*tight*) selections and passing less restrictive *loose* selections can be used to estimate the number of fake leptons in the dilepton data sample, if the probability for a lepton passing the loose selections to also pass the tight selections is known. This probability, referred to as the tight-to-loose (TL) ratio, is measured in data in an independent sample dominated by multijet production events with a single lepton passing loose selections. Assuming that the chance to pass or fail the tight selections is independent between two lepton candidates, counts of events with none, one, and two leptons failing the tight selections can be used to determine the number of events with two prompt leptons, one fake, and two fake leptons. The TL ratio method is used for estimates of fake electrons, muons, and hadronic taus.

While the tight selections of leptons are fixed by the definitions of the baseline and search regions, the loose selections can vary. Two sets of loose selections are used in the TL ratio method for electrons and muons, later referred to as method (A1) and (A2). The two loose selections for muons are (A1) defined by relaxing I_{rel} to be < 0.4 and relaxing the requirement for the lepton to originate from the interaction vertex; (A2) defined by $I_{\mathrm{rel}} < 1.0$. The two loosened selections for electrons are (A1) $I_{\mathrm{rel}} < 0.6$; (A2) $I_{\mathrm{rel}} < 1.0$ (0.6) for electrons with $|\eta| < 1.5$ (> 1.5) with a relaxed identification requirement. The values of the TL ratio are in the range of 0.2–0.3 for electrons and muons using method (A1), and about a factor of two lower using method (A2). As a reference, the estimates in the baseline *high-p_{T} dilepton* selections for the (A1) loose selections yield 14 ± 2, 14 ± 2, and 30 ± 4 and, similarly for (A2), 11.1 ± 1.5, 16.1 ± 1.4, and 26 ± 2 in the ee, $\mu\mu$, and eμ final state, respectively, where the uncertainties are statistical only. The contribution from two fake leptons is less than 20% of the total number

of events with fake leptons. In this and other cases the two TL ratio methods give consistent results. The systematic uncertainty is estimated based on applying the TL ratio method to simulated events, varying the TL ratio from the nominal in events with higher or lower jet activity and varying the heavy flavor content in the control sample. The combined systematic uncertainty on the method, shared by both (A1) and (A2), is approximately 50%, in agreement with earlier estimates [9].

Two more methods are developed for estimates of the contribution with fake leptons in events passing the *inclusive dilepton* selection, later collectively referred to as method (B). The number of events with two fake leptons is computed assuming a factorization of the isolation and $E_{\mathrm{T}}^{\mathrm{miss}}$ requirements. The probability for each lepton (separately) to pass the isolation requirement and, separately, for the event to pass the $E_{\mathrm{T}}^{\mathrm{miss}}$ requirement can be multiplied to get a combined probability for the event to pass these requirements. The contribution with two fake leptons is thus given by the number of events not required to pass the $E_{\mathrm{T}}^{\mathrm{miss}}$ or lepton isolation selections scaled by this combined probability. The systematic uncertainty is estimated based on tests of this method in simulation and in control data samples. In the baseline *inclusive dilepton* selections 0.7 ± 0.7, 7 ± 3, and 5 ± 4 events with two fake leptons are expected in the ee, $\mu\mu$, and eμ final states, respectively, reported with the systematic and statistical uncertainties combined. As a comparison, consistent estimates are obtained using the TL ratio method (A1), with, correspondingly, 0.3 ± 0.3, 7 ± 4, and 2.6 ± 1.5 events expected.

Events with one fake lepton are estimated for the *inclusive dilepton* selections with the method (B) using events with one of the two leptons failing the isolation requirement, as follows. The isolation distribution of fake leptons is measured as a function of the lepton momentum and the number of jets using a sample of events enriched with $\mathrm{b\bar{b}}$ production in data. The isolation variable shape is reweighted to the expected distribution of the lepton momentum and the number of jets in a simulated $\mathrm{t\bar{t}}$ sample. The fraction of the reweighted shape with $I_{\mathrm{rel}} < 0.15$ gives the expected efficiency of this isolation requirement for fake leptons in events with two leptons. The average efficiency is found to be 0.039 ± 0.001 and 0.068 ± 0.004 for muons and electrons, respectively. The systematic uncertainty of approximately 50 (30)% for electrons (muons) is estimated based on the tests of this method in simulation as well as from the observed dependence of the estimated efficiency on event kinematics and residual contribution from W or Z events. The estimate of events with one fake lepton passing the baseline selection is 5 ± 3, 15 ± 7, and 18 ± 8 for ee, $\mu\mu$, and eμ, respectively, reported with the systematic and statistical uncertainties combined. The predictions of the TL ratio method (A1) for these events are 9 ± 5, 12 ± 7, and 20 ± 11 in the ee, $\mu\mu$, and eμ final states.

The estimates of the number of events with fake taus are based on the TL ratio method. The nominal tau selections described in Section 3 are the *tight* selections. The *loose* selections are defined by relaxing the isolation requirement and a requirement that at least one of the hadronic decay modes is reconstructed [15]. The tau fake TL ratio is measured as a function of the tau p_{T} and $|\eta|$ in multijet data collected with triggers which require jets with $H_{\mathrm{T}} > 150$ or 200 GeV. The measured value decreases with p_{T}, varying from 0.2 to 0.03. A combined systematic uncertainty on the prediction of the number of events with fake taus is estimated by combining variations of the prediction due to variations of the TL ratio as well as from tests of the method in simulation. The TL ratio changes are tested with different H_{T} regions, modified definition of the loose taus, and different binning of the measurement in p_{T} and $|\eta|$. The combined systematic uncertainty on the total number of events with fake taus is 70% in the baseline selection region, and 80% in the search region 1. The number of events with fake taus passing the baseline selections is predicted to be $2.2 \pm 0.1 \pm 1.2$, $4.0 \pm 0.9 \pm 3.1$, and $0.2 \pm 0.3 \pm 0.1$ in the eτ, $\mu\tau$, and $\tau\tau$ events, respectively, where the statistical and systematic uncertainties are displayed

separately.

6.2 Lepton charge misreconstruction

Contribution from events with lepton charge misreconstruction arises from abundant SM sources with oppositely charged lepton pairs with at least one electron or tau. The contribution from muon charge misreconstruction is negligible: it is much smaller than that for electrons or taus, and is also much smaller than other backgrounds in the dimuon final state.

Charge misreconstruction for electrons occurs due to radiation processes in the tracker; it depends on the electron pseudorapidity due to differences in the amount of material in the tracker. It also increases with the electron momentum due to loss in resolution in the tracker. The charge misreconstruction probability f_q^e is measured in simulated events as a function of electron pseudorapidity and momentum. For electrons from Z production, the average value of f_q^e is approximately 2×10^{-4} (3×10^{-3}) in the ECAL barrel $|\eta| < 1.5$ (in the ECAL endcap $|\eta| > 1.5$), as extracted from events in data, in agreement with expectation from simulation. In events selected with same-sign electron pairs with at least one electron $p_T > 20$ GeV/c and the other $p_T > 10$ GeV/c in an invariant mass range of 76–106 GeV we find 129 events in data, compared to 94 ± 10 Z events expected in simulation, 100.0 ± 0.3 expected from the oppositely-charged dielectron events weighted by f_q^e, and 8 ± 4 events expected to be from fake electrons. Based on this observation, we apply a correction factor of 1.2 to the expected number of events with misreconstructed electron charge. Alternatively, the f_q^e is measured directly in data using the limited sample of Z events. Consistent results are found for the estimates of the number of events with electrons with misreconstructed charge in the baseline and search regions considered. The total contribution is less than 10% of all other backgrounds. The systematic uncertainty of the estimates is approximately 20%, based on the uncertainty from the comparison with the Z events as well as expected differences in the f_q^e for p_T and η in Z events and typical background events like $t\bar{t}$.

Tau charge is determined as the sum of the charge of the hadrons associated with the tau decay. In the three prong decay of a tau, charge misreconstruction occurs when a track from background is associated with the products of the tau decay. The tau charge misreconstruction probability f_q^τ is expected to be more than an order of magnitude higher than that for electrons, as predicted by simulation. It is estimated to be approximately $7.1 \pm 1.0(\text{stat.}) \pm 2.5(\text{syst})\%$ for taus from Z decays in data events, where the statistical and systematic uncertainties are shown separately. A systematic uncertainty on f_q^τ of 35% is dominated by the uncertainty on the QCD multijet background shape, and also includes subdominant contributions from the method of extracting the number of signal events, and the uncertainty on the signal fitting procedure. The ratio of the f_q^τ measured in data to the value measured in simulation is 2.4 ± 0.9, where the uncertainty includes statistical and systematic components. In events passing the baseline or tighter selections considered here, the contribution from taus with misreconstructed charge is less than 40%.

7 Signal Acceptance and Efficiency Systematic Uncertainties

Electron and muon trigger, identification, and reconstruction efficiencies are measured in data using $Z \to ee$ and $\mu\mu$ events and are then compared to simulation to measure simulation-to-data corrections. The uncertainty on the combined lepton selection efficiency above $p_T \approx 20$ GeV is known at the level of approximately 3% per lepton. The uncertainties increase as the efficiencies themselves decrease towards lower p_T, reaching 5% per muon at 5 GeV (electron at

10 GeV). In addition, there is a potential mismodeling of the lepton isolation efficiency between data and simulation that grows with the amount of hadronic activity per event. To assess this, we compare the isolation efficiency as a function of track multiplicity in data and simulation for $Z \to ee$ and $\mu\mu$, and extrapolate to new physics signals with large hadronic activity using simulation, as discussed in more detail in Section 9. Based on this, we assign an additional 5% systematic uncertainty per lepton.

The τ reconstruction efficiency can not be studied at the same level of detail in data as for electrons and muons, and we depend to a greater extent on accurate simulation. We assign an uncertainty of 10% [12] to the combined selection and reconstruction efficiency of τ. Lepton selection efficiency values enter the simplified model of signal event selection efficiency, as discussed in Section 9.

There is also a 5% uncertainty associated with the efficiency of the H_T requirement (and E_T^{miss} for *τ-dileptons*) in triggers that have this requirement. This uncertainty is dominated by the statistical uncertainty in the samples used to measure the efficiency at high values of H_T (or E_T^{miss}) and dependence of the measured efficiency at low values. The uncertainty of 5% is a conservative value for search region 1.

An additional source of systematic uncertainty is associated with the uncertainty on the hadronic energy scale [26, 27], estimated to be in the range of 2–5% per jet as a function of jet kinematics. This uncertainty is degraded by an uncertainty due to multiple interactions (pileup) decreasing inversely proportionally to the jet p_T, with a value of 5% for 40 GeV jets. Finally, a 5% uncertainty is added to account for other differences between the current data sample and that of Refs. [26, 27]. A combined uncertainty of 7.5% is used conservatively for all jets considered in the analysis. This scale uncertainty limits our understanding of the efficiency of the H_T and E_T^{miss} requirements. This uncertainty corresponds to an uncertainty of 3% on the number of expected events passing the most stringent selection, that of search region 1 with $H_T > 400$ GeV and $E_T^{miss} > 120$ GeV, computed for the LM6 benchmark point. To cover models with less energetic jets in the final state, we assign an uncertainty of 5%.

Based on the estimates in Ref. [9], uncertainties in the acceptance due to the modeling of initial- and final-state radiation and knowledge of the parton density functions (PDF) are estimated to be 2%.

Based on LM6 as a signal model, we arrive at total uncertainties on signal efficiencies of 14%, 17%, and 20% for search region 1 in the *high-p_T*, *inclusive*, and *τ dilepton* categories, respectively. This includes a 6% systematic uncertainty on the integrated luminosity [28]. In addition, to interpret these limits in terms of constraints on new physics models, one needs to take into account any model-dependent theoretical uncertainties.

8 Results

As discussed in Section 5, a baseline selection region was defined for each of the three dilepton categories (*inclusive*, *high-p_T*, and τ) in order to assess the performance of the background prediction methods outlined in Section 6 with a statistically meaningful event sample. By design, the chosen search regions cannot serve this purpose, as they are not expected to be populated by many background events. A summary of the background predictions together with the number of observed events is provided for each channel in the three baseline selection regions in Table 1. For the *inclusive* and *high-p_T dilepton* selections, two sets of complimentary methods, (B)+(A1) and (A1)+(A2) respectively, are used to measure the backgrounds, and these compare

well with one another, providing mutually consistent background predictions. A visual summary of these comparisons for the baseline region is given in Fig. 3. In all baseline regions good agreement with the observed yields is demonstrated, establishing that the backgrounds can be reliably estimated within the combined statistical and systematic uncertainties. The systematic uncertainty on the estimates of the number of fake leptons is the dominant uncertainty in all channels; it is correlated among different channels, which is reflected in the uncertainty on the total being approximately equal to the sum of uncertainties in each channel.

Table 1: Observed number of events in data compared to the predicted background yields for the *inclusive*, *high-p_T*, and τ dilepton baseline regions. The net predicted yields, differing in estimates of the fake lepton contributions using methods (A1), (A2), and (B), are shown separately. The uncertainties include the statistical and systematic components added in quadrature.

Baseline region	ee	$\mu\mu$	eμ	Total
Inclusive dileptons				
Predicted background by (B)	7 ± 3	23 ± 5	26 ± 7	56 ± 18
Predicted background by (A1)	11 ± 5	21 ± 10	26 ± 12	58 ± 26
Observed	7	23	19	49
High-p_T dileptons				
Predicted background by (A1)	19 ± 8	18 ± 8	38 ± 17	75 ± 32
Predicted background by (A2)	16 ± 6	19 ± 8	32 ± 13	67 ± 27
Observed	16	16	24	56
Baseline region	$e\tau$	$\mu\tau$	$\tau\tau$	Total
τ dileptons				
Predicted background	3.3 ± 1.3	5.7 ± 3.3	0.4 ± 0.4	9.3 ± 4.6
Observed	4	7	0	11

The results of our searches are summarized in Tables 2, 3, and 4 for the *inclusive*, *high-p_T*, and *τ dilepton* selections. The background predictions are shown with statistical and systematic uncertainties combined. Here the statistical component of the uncertainty is more significant and the uncertainty on the total of all channels is less than a simple sum of uncertainties. Again, for the *inclusive* and *high-p_T dilepton* selections, two complimentary background predictions are provided.

We see no evidence of an event yield in excess of the background predictions and set 95% CL upper limits (UL) on the number of observed events using a hybrid frequentist-bayesian CL_s method [29] with nuisance parameters and the signal strength maximizing the ratio of the signal-with-background and background-only likelihoods. Log-normal distributions are used for the efficiency and background uncertainties. The limits are presented in the final column of Tables 2, 3, and 4. In the case where two methods were executed to predict the backgrounds, the more conservative limit is quoted. The limits include uncertainties on the signal efficiency of 14%, 17%, and 20% for the *inclusive*, *high-p_T*, and *τ dilepton* selections, respectively, which are discussed in more detail in Section 7.

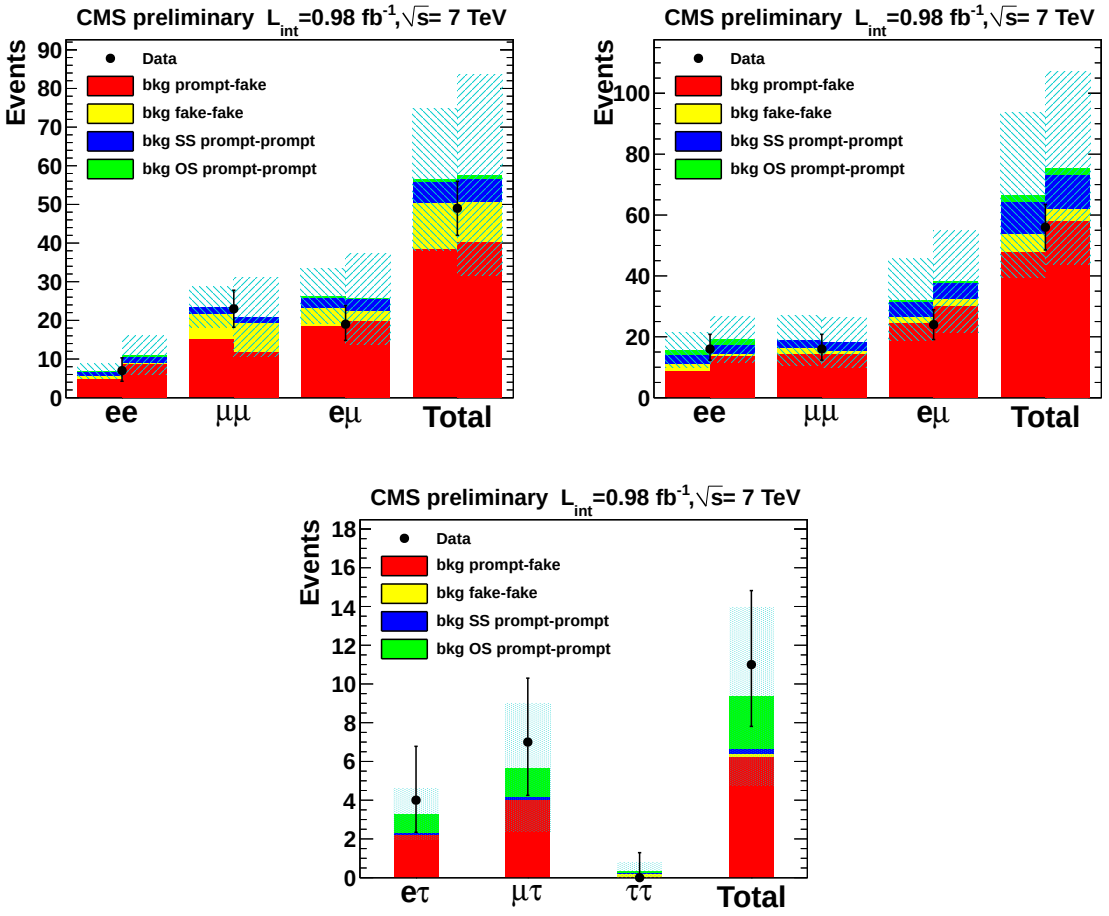

Figure 3: Summary of background predictions and observed yields in the baseline region for the *inclusive* (left), *high-p_T* (right), and τ *dilepton* (bottom) selections. For the *inclusive* selections, the results of method (B) are compared with those from method (A1) in the left and right bar for each channel, respectively. For the *high-p_T* selections, the results of method (A2) are compared with those from method (A1) in the left and right bar for each channel, respectively. Predictions for events with one and two fakes (prompt-fake and fake-fake), contributions from simulated backgrounds (SS prompt-prompt), and those from events with a lepton charge misreconstruction (OS prompt-prompt) are reported separately.

Table 2: Observed number of events in data compared to the predicted background yields for the *inclusive dilepton* search regions. The net predicted yields, differing in estimates of the fake lepton contributions using methods (A1), and (B), are shown separately. The uncertainties include the statistical and systematic components added in quadrature. The last column (95% CL UL yield) represents observed upper limits on event yields from new physics.

Search region (minimum $H_T / E_{\mathrm{T}}^{\mathrm{miss}}$)	ee	$\mu\mu$	eμ	Total	95% CL UL yield
Region 1 (400/120)					
Predicted background by (B)	0.2 ± 0.1	0.9 ± 0.3	0.9 ± 0.3	2.0 ± 0.7	
Predicted background by (A1)	0.4 ± 0.4	1.2 ± 0.8	0.7 ± 0.4	2.3 ± 1.2	
Observed	0	1	0	1	3.7
Region 2 (400/50)					
Predicted background by (B)	1.0 ± 0.4	2.3 ± 0.7	3.0 ± 1.0	6.2 ± 2.2	
Predicted background by (A1)	1.3 ± 0.7	2.5 ± 1.5	1.4 ± 0.7	5.3 ± 2.4	
Observed	1	4	2	7	8.9
Region 3 (200/120)					
Predicted background by (B)	0.8 ± 0.4	3.6 ± 1.3	3.4 ± 1.3	7.8 ± 2.9	
Predicted background by (A1)	1.5 ± 0.9	3.0 ± 1.6	2.1 ± 1.0	6.6 ± 2.9	
Observed	0	4	2	6	7.3

Table 3: Observed number of events in data compared to the predicted background yields for the *high-p_T* search regions. The net predicted yields, differing in estimates of the fake lepton contributions using methods (A1), and (A2), are shown separately. The uncertainties include the statistical and systematic components added in quadrature. The last column (95% CL UL yield) represents observed upper limits on event yields from new physics.

Search Region (minimum $H_T / E_{\mathrm{T}}^{\mathrm{miss}}$)	ee	$\mu\mu$	eμ	Total	95% CL UL yield
Region 1 (400/120)					
Predicted background by (A1)	0.4 ± 0.3	0.4 ± 0.3	0.7 ± 0.4	1.4 ± 0.7	
Predicted background by (A2)	0.7 ± 0.5	0.4 ± 0.3	0.4 ± 0.3	1.4 ± 0.7	
Observed	0	0	0	0	3.0
Region 2 (400/50)					
Predicted background by (A1)	1.4 ± 0.8	1.3 ± 0.8	1.3 ± 0.6	4.0 ± 1.7	
Predicted background by (A2)	1.5 ± 0.8	0.8 ± 0.4	1.0 ± 0.5	3.3 ± 1.2	
Observed	1	2	2	5	7.5
Region 3 (200/120)					
Predicted background by (A1)	1.2 ± 0.7	1.5 ± 0.8	1.8 ± 0.8	4.5 ± 1.9	
Predicted background by (A2)	1.3 ± 0.7	1.8 ± 0.8	1.8 ± 0.7	4.9 ± 1.8	
Observed	0	2	1	3	5.2
Region 4 (80/100)					
Predicted background by (A1)	2.5 ± 1.2	2.6 ± 1.2	4.9 ± 2.2	10 ± 4	
Predicted background by (A2)	2.4 ± 1.0	3.6 ± 1.6	4.4 ± 1.6	10 ± 4	
Observed	3	2	2	7	6.0

Table 4: Observed number of events in data compared to the predicted background yields for the τ *dilepton* search region. The uncertainties include the statistical and systematic components added in quadrature. The last column (95% CL UL yield) represents the observed upper limit on event yields from new physics.

Search Region (minimum $H_T / E_{\mathrm{T}}^{\mathrm{miss}}$)	$e\tau$	$\mu\tau$	$\tau\tau$	Total	95% CL UL yield
Region 1 (400/120)					
Predicted background	1.1 ± 0.4	1.8 ± 1.4	0.0 ± 0.2	2.9 ± 1.7	
Observed	1	2	0	3	5.8

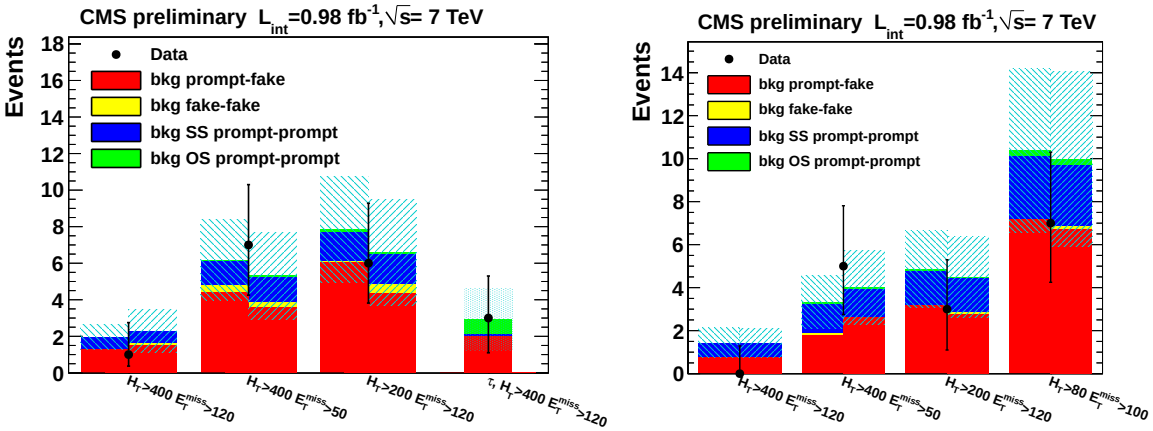

Figure 4: Summary of background predictions and observed yields in the search regions for the *inclusive* and τ (left), and *high-p_T dilepton* (right) selections. For the *inclusive* selections, the results of method (B) are compared with those from method (A1) in the left and right bar for each channel, respectively. For the *high-p_T* selections, the results of method (A2) are compared with those from method (A1) in the left and right bar for each channel, respectively. Predictions for events with one and two fakes (prompt-fake and fake-fake), contributions from simulated backgrounds (SS prompt-prompt), and those from events with a lepton charge misreconstruction (OS prompt-prompt) are reported separately.

As a reference to the limits set in Tables 2, 3, and 4 in search region 1, the most restrictive one, with $H_T > 400$ GeV and $E_T^{miss} > 120$ GeV, we obtain 3.9 (5.1), 3.6 (4.7), and 0.6 (0.8) events expected in the benchmark LM6 model, considering the cross section of 0.31 (0.4) pb computed at the leading (next-to-leading) order. Considering the next-to-leading order cross section, this model point is excluded by this analysis in either the *inclusive* or the *high-p_T dilepton* selections.

9 Interpretation of Results

One of the challenges of signature-based searches is to convey information in a form that can be used to test a variety of specific physics models. We have presented in Ref. [9] additional information that can be used to confront models of new physics in an approximate way by generator-level simulation studies. The approximate model of lepton, jet, and E_T^{miss} selection efficiency in terms of the generator level quantities was shown to be sufficiently precise to reproduce the constraints on new physics models that otherwise would require full CMS detector simulation.

We confirm here the main features of the model presented in the original work and update the results of the parameterization of the leptons, E_T^{miss}, and H_T selection efficiency curves as a function of the generator level quantities using events in LM6 benchmark model. All of the general features remain with overall changes affecting the combined efficiency by less than 10%.

The efficiency dependence can be parameterized as a function of p_T as $\epsilon_\infty\{\text{erf}[(p_T - C)/\sigma]\} + \epsilon_C\{1 - \text{erf}[(p_T - C)/\sigma]\}$, where ϵ_∞ gives the value of efficiency plateau at high momenta, C is equal to 5 (10) for muons (electrons), ϵ_C gives the value of the efficiency at $p_T = C$, and σ describes how fast the transition region is. The parameterization is summarized in Table 5 for electrons and muons. Tau selection efficiency fits a slightly different shape $\epsilon_\infty\{1 - \exp[-\alpha(p_T - C)]\}$, where the parameters ϵ_∞, α, and C are equal to 0.34, 0.052, and 15, respectively.

Table 5: Parameterization of the electron and muon selection efficiencies using the function described in text.

Parameter	Electrons	Muons
C, (GeV)	10	5
ϵ_∞	0.68	0.74
ϵ_C	0.19	0.24
σ, (GeV)	19	15

The efficiency for an event to pass a given reconstructed E_T^{miss} (H_T) threshold is studied as a function of the generator level E_T^{miss} (H_T) in events passing generator level $H_T > 200$ GeV ($E_T^{miss} > 30$ GeV). The dependences are parameterized by $0.5\epsilon_\infty\{\text{erf}[(x - x_{1/2})/\sigma] + 1\}$, where x corresponds to the generator level E_T^{miss} or H_T, and ϵ_∞ is the selection efficiency plateau at high values of x. Neither the E_T^{miss} nor H_T show a significant bias in the position of the point with half the plateau efficiency ($x_{1/2}$). The inefficiency at the plateau is essentially negligible. The width of the threshold σ increases with the value of the cut.

Table 6: Summary of parameters of the function $0.5\epsilon_\infty\{\mathrm{erf}[(x - x_{1/2})/\sigma] + 1\}$ used to characterize the H_T and $E_\mathrm{T}^\mathrm{miss}$ selection efficiency.

Parameter	H_T		$E_\mathrm{T}^\mathrm{miss}$		
	> 200 GeV	> 400 GeV	> 50 GeV	> 100 GeV	> 120 GeV
ϵ_∞	0.998	0.987	0.998	0.997	0.999
$x_{1/2}$, (GeV)	193	379	46	100	121
σ, (GeV)	87	113	33	37	40

As a reference to other searches for SUSY, we interpret results in search region 1 in the context of CMSSM model. The observed upper limits on the number of signal events reported in Section 8 are compared to the expected number of events in the CMSSM model in a plane of $(m_0, m_{1/2})$ for $\tan\beta = 10$, $A_0 = 0$, and $\mu > 0$. All points with mean expected values above this upper limit are interpreted as excluded at the 95% CL. The observed exclusion region for the *high-p_T dilepton* selection is displayed in Fig. 5. The shaded region represents the uncertainty on the position of the limit due to an uncertainty on the production cross section of CMSSM resulting from PDF uncertainties and the NLO cross section uncertainty estimated from varying the renormalization scale by a factor of two. The expected exclusion region is approximately the same as the observed one. An exclusion region based on our previous analysis [9] is also shown for a comparison. The new result extends to gluino masses of 825 GeV in the region with similar values of squark masses and extends to gluino masses of 675 GeV for higher squark masses. This can be compared to the exclusion of just around 500 GeV in the previous analysis. The result for the *inclusive dilepton* selection is also shown in Fig. 6.

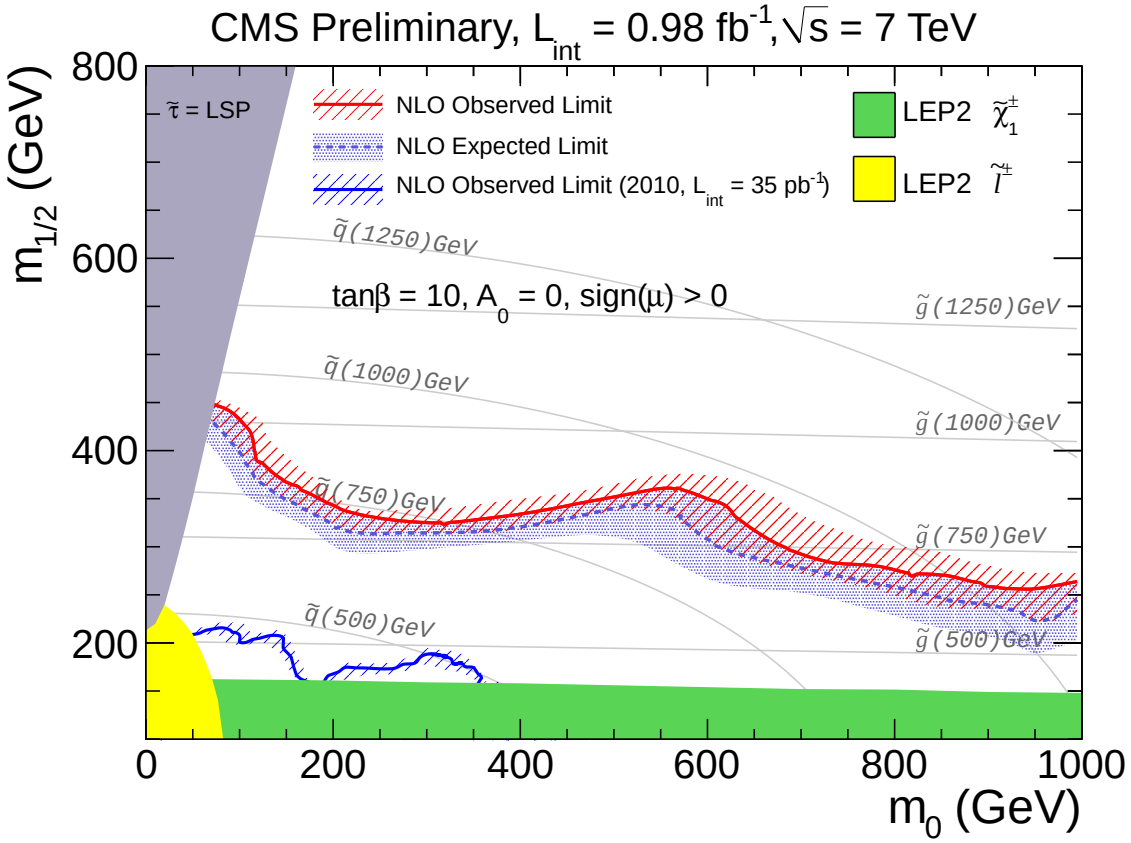

Figure 5: Exclusion region in the CMSSM corresponding to the observed upper limit of 3.0 events in the search region 1 of the *high-p_T dilepton* selections. The result of the previous analysis [9] is shown to illustrate the improvement since.

10 Summary and Conclusions

We have searched for new physics with same-sign dilepton events in the ee, $\mu\mu$, eμ, eτ, $\mu\tau$, and $\tau\tau$ final states, and have seen no evidence for an excess over the background prediction. The τ leptons referred to here are reconstructed via their hadronic decays.

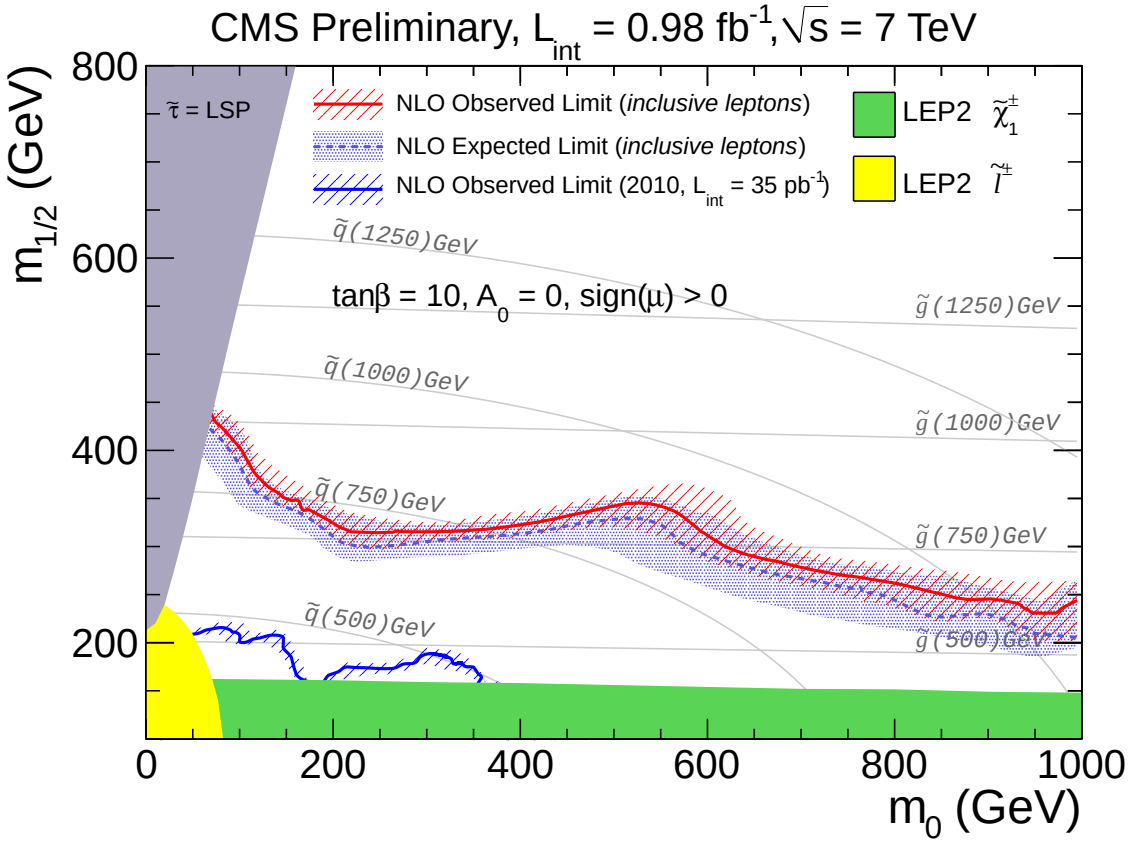

Figure 6: Exclusion region in the CMSSM corresponding to the observed upper limit of 3.7 events in the search region 1 of the *inclusive dilepton* selections. The result of the previous analysis [9] is shown to illustrate the improvement since.

The dominant background processes in all final states except $\tau\tau$ involve events with one fake lepton. In the $\tau\tau$ final state, events with two fake τ dominate. We have presented methods to derive estimates for all major background sources from the data. We have set 95% CL upper limits on the number of signal events within $|\eta| < 2.4$ at 0.98 fb^{-1} in the range of 3.0 to 8.9 events, depending on signal search region. As a reference to other SUSY searches, we report exclusion regions in the CMSSM parameter space.

References

[1] R. Barnett, J. Gunion, and H. Haber, "Discovering supersymmetry with like sign dileptons", *Phys. Lett.* **B 315** (1993) 349. doi:10.1016/0370-2693(93)91623-U.

[2] M. Guchait and D. P. Roy, "Like sign dilepton signature for gluino production at the CERN LHC including top quark and Higgs boson effects", *Phys. Rev.* **D 52** (1995) 133. doi:10.1103/PhysRevD.52.133.

[3] H. Baer et al., "Signals for minimal supergravity at the CERN Large Hadron Collider II: Multilepton channels", *Phys. Rev.* **D 53** (1996) 6241. doi:10.1103/PhysRevD.53.6241.

[4] H. Cheng, K. Matchev, and M. Schmaltz, "Bosonic supersymmetry? Getting fooled at the CERN LHC", *Phys. Rev.* **D 66** (2002) 056006. doi:10.1103/PhysRevD.66.056006.

[5] R. Contino and G. Servant, "Discovering the top partners at the LHC using same-sign dilepton final states", *JHEP* **06** (2008) 026. doi:10.1088/1126-6708/2008/06/026.

[6] F. Almeida et al., "Same-sign dileptons as a signature for heavy Majorana neutrinos in hadron-hadron collisions", *Phys. Lett.* **B 400** (1997) 331. doi:10.1016/S0370-2693(97)00143-3.

[7] Y. Bai and Z. Han, "Top-antitop and Top-top Resonances in the Dilepton Channel at the CERN LHC", *JHEP* **04** (2009) 056. doi:10.1088/1126-6708/2009/04/056.

[8] G. Bertone, D. Hooper, and J. Silk, "Particle dark matter: Evidence, candidates and constraints", *Phys. Rept.* **405** (2005) 279. doi:10.1016/j.physrep.2004.08.031.

[9] CMS Collaboration, "Search for new physics with same-sign isolated dilepton events with jets and missing transverse energy at the LHC", arXiv:1104.3168. To be published in *JHEP*.

[10] CMS Collaboration, "The CMS experiment at the CERN LHC", *JINST* **3** (2008) S08004. doi:10.1088/1748-0221/3/08/S08004.

[11] CMS Collaboration, "Measurements of Inclusive W and Z Cross Sections in pp Collisions at $\sqrt{s} = 7$ TeV", *JHEP* **01** (2011) 080. doi:10.1007/JHEP01(2011)080.

[12] CMS Collaboration, "Performance of tau reconstruction algorithms in 2010 data collected with CMS", *CMS Physics Analysis Summary* **CMS-PAS-TAU-11-001** (2011).

[13] CMS Collaboration, "Performance of muon identification in pp collisions at $\sqrt{s}$ = 7 TeV", *CMS Physics Analysis Summary* **CMS-PAS-MUO-10-002** (2010).

[14] CMS Collaboration, "Electron reconstruction and identification at $\sqrt{s}$=7 TeV", *CMS Physics Analysis Summary* **CMS-PAS-EGM-10-004** (2010).

[15] CMS Collaboration, "Study of tau reconstruction algorithms using pp collisions data collected at $\sqrt{s} = 7$ TeV with CMS detector at LHC", *CMS Physics Analysis Summary* **CMS-PAS-PFT-10-004** (2010).

[16] CMS Collaboration, "Particle–Flow Event Reconstruction in CMS and Performance for Jets, Taus, and $E_{\mathrm{T}}^{\mathrm{miss}}$", *CMS Physics Analysis Summary* **CMS-PAS-PFT-09-001** (2009).

[17] CMS Collaboration, "Commissioning of the Particle-Flow Reconstruction in Minimum-Bias and Jet Events from pp Collisions at 7 TeV", *CMS Physics Analysis Summary* **CMS-PAS-PFT-10-002** (2010).

[18] M. Cacciari, G. Salam, and G. Soyez, "The anti-k_T jet clustering algorithm", *JHEP* **04** (2008) 063. doi:10.1088/1126-6708/2008/04/063.

[19] CMS Collaboration, "Jets in 0.9 and 2.36 TeV pp Collisions", *CMS Physics Analysis Summary* **CMS-PAS-JME-10-001** (2010).

[20] CMS Collaboration, "Jet Performance in pp Collisions at $\sqrt{s}$=7 TeV", *CMS Physics Analysis Summary* **CMS-PAS-JME-10-003** (2010).

[21] CMS Collaboration, "Search for Neutral Higgs Bosons Decaying to Tau Pairs in pp Collisions at $\sqrt{s} = 7$ TeV", *CMS Physics Analysis Summary* **CMS-PAS-HIG-11-009** (2011).

[22] G. Kane et al., "Study of constrained minimal supersymmetry", *Phys. Rev.* **D 49** (1994), no. 11, 6173. doi:10.1103/PhysRevD.49.6173.

[23] N. Arkani-Hamed, L. J. Hall, H. Murayama et al., "Small neutrino masses from supersymmetry breaking", *Phys. Rev.* **D64** (2001) 115011, arXiv:hep-ph/0006312. doi:10.1103/PhysRevD.64.115011.

[24] G. Belanger, S. Kraml, and A. Lessa, "Light Sneutrino Dark Matter at the LHC", arXiv:1105.4878.

[25] ATLAS Collaboration, "Measurement of the WZ $\to \ell\ell\ell\nu$ Production Cross Section in Proton-Proton Collisions at $\sqrt{s} = 7$ TeV with the ATLAS Detector", *ATLAS conference report* **ATLAS-CONF-2011-084** (2011).

[26] CMS Collaboration, "Jet Energy Corrections determination at 7 TeV", *CMS Physics Analysis Summary* **CMS-PAS-JME-10-010** (2010).

[27] CMS Collaboration, "On measuring transverse energy with the CMS detector in pp collisions at $\sqrt{s} = 7$ TeV", *CMS Paper in Preparation* **CMS-PAPER-JME-10-009** (2010).

[28] CMS Collaboration, "Absolute luminosity normalization", *CMS Detector Performance Summary* **CMS-DP-2011-003** (2011). The value of 4% is inflated to 6%, based on observations in 2011 data sample.

[29] Particle Data Group Collaboration, "Review of particle physics", *J. Phys.* **G 37** (2010) 075021. doi:10.1088/0954-3899/37/7A/075021.

A Supporting material useful for presentations

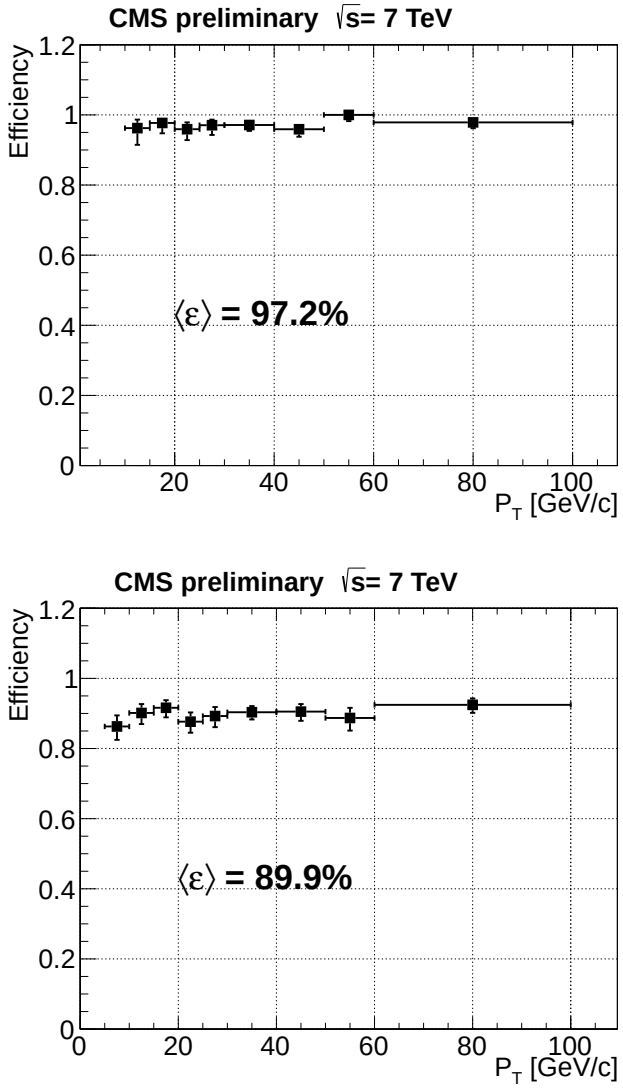

Figure 7: Efficiency of the dielectron (top) and dimuon (bottom) trigger selection for the *inclusive dilepton* final states. The efficiency is measured with respect to leptons passing all identification and isolation requirements. It is displayed as a function of the lower lepton momentum in the pair. The dielectron (dimuon) trigger selection has a higher (lower) efficiency compared to that of the electron-muon trigger.

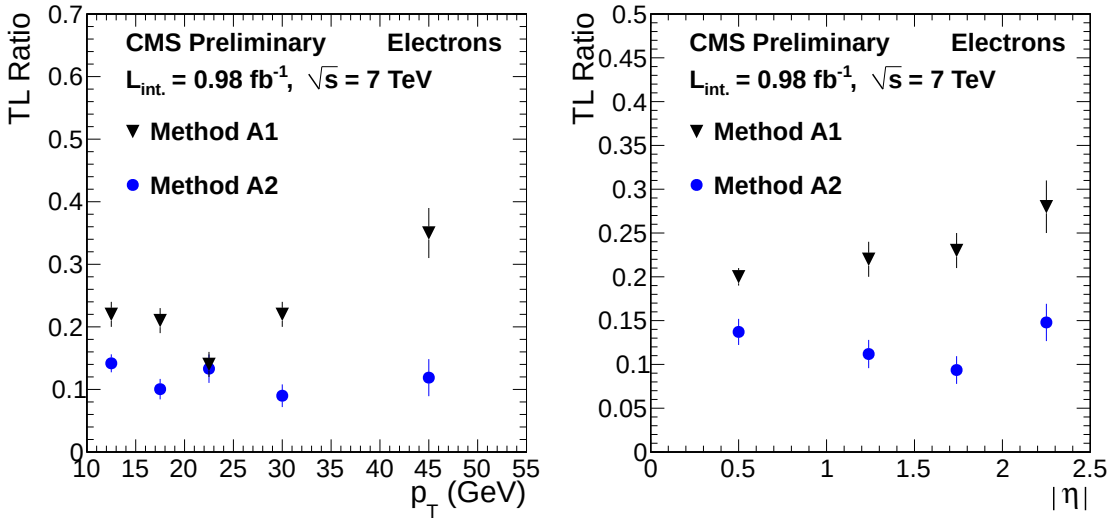

Figure 8: Electron TL ratio projected on p_{T} (left) and $|\eta|$ (right) as measured using method (A1) and (A2). The measurement is done for electrons up to 55 GeV/c.

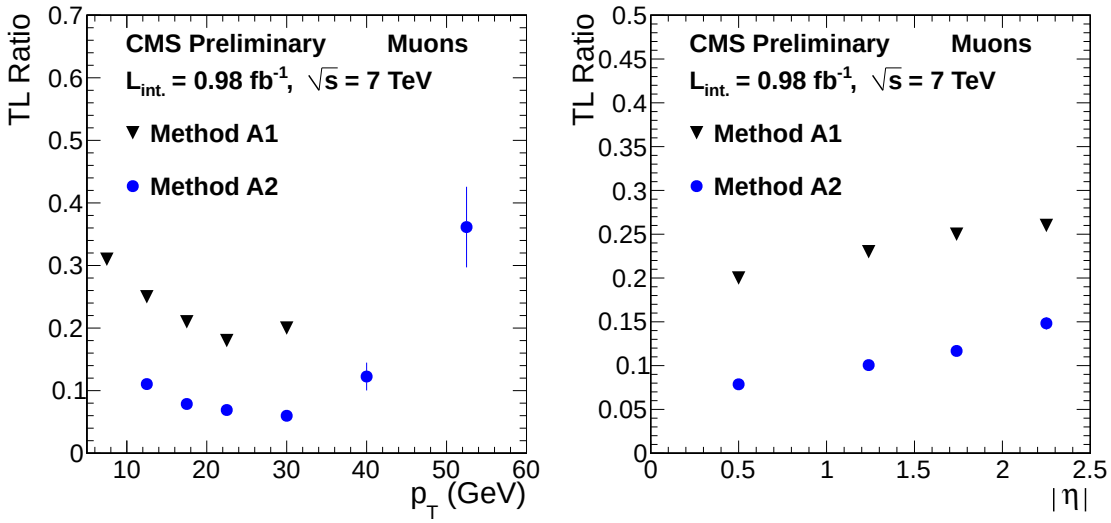

Figure 9: Muon TL ratio projected on p_{T} (left) and $|\eta|$ (right) as measured using method (A1) and (A2). The measurement by (A1) is done for muons up to 35 GeV/c.

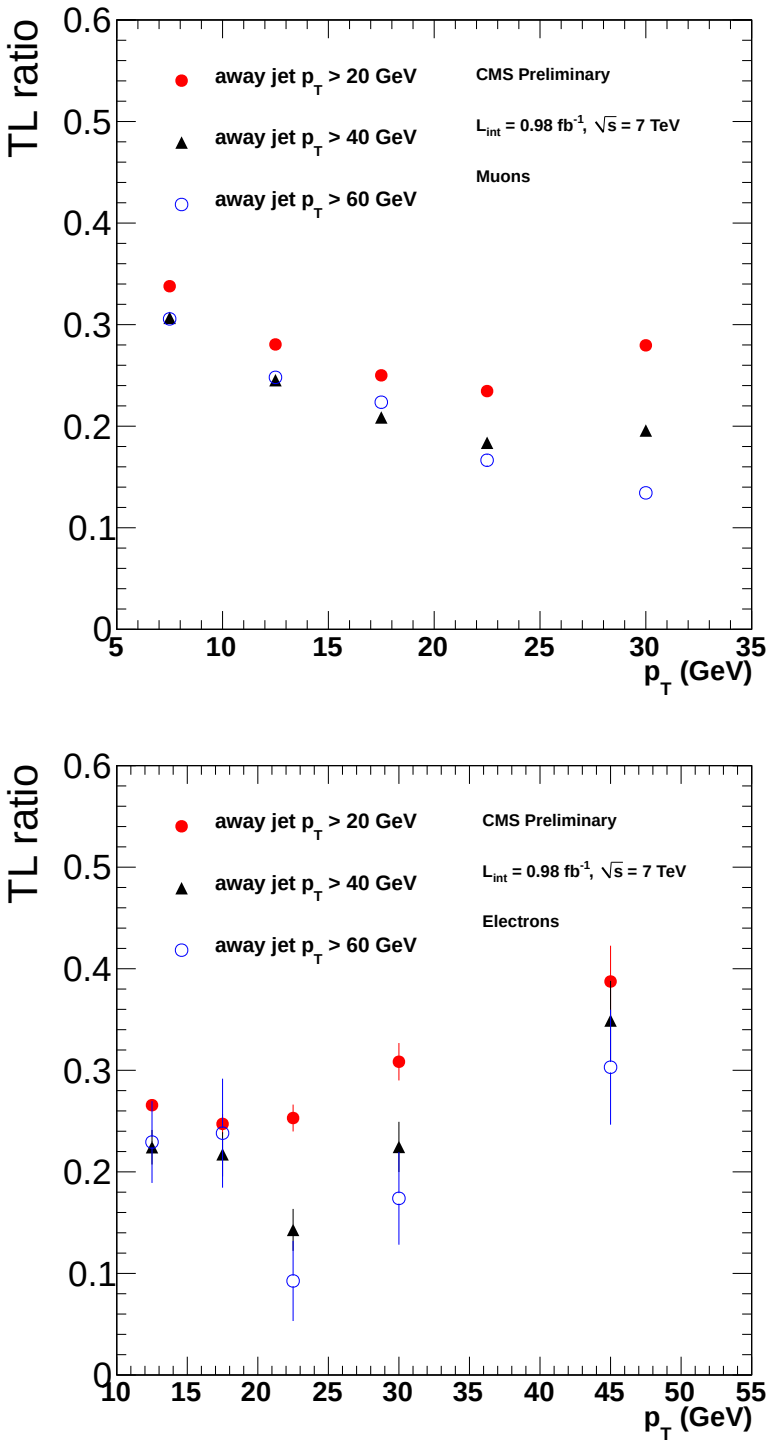

Figure 10: Muon (left) and electron (right) TL ratio projected on p_{T} using method (A1). The TL ratio distribution is displayed separately for events with a jet separated from the lepton candidate by $\Delta R > 1$ and the jet required to have p_{T} above 20, 40, and 60 GeV. The central value is measured for the case with a jet $p_{\mathrm{T}} > 40$ GeV, while the range of values measured with other jet requirements represents an estimate of the systematic uncertainty.

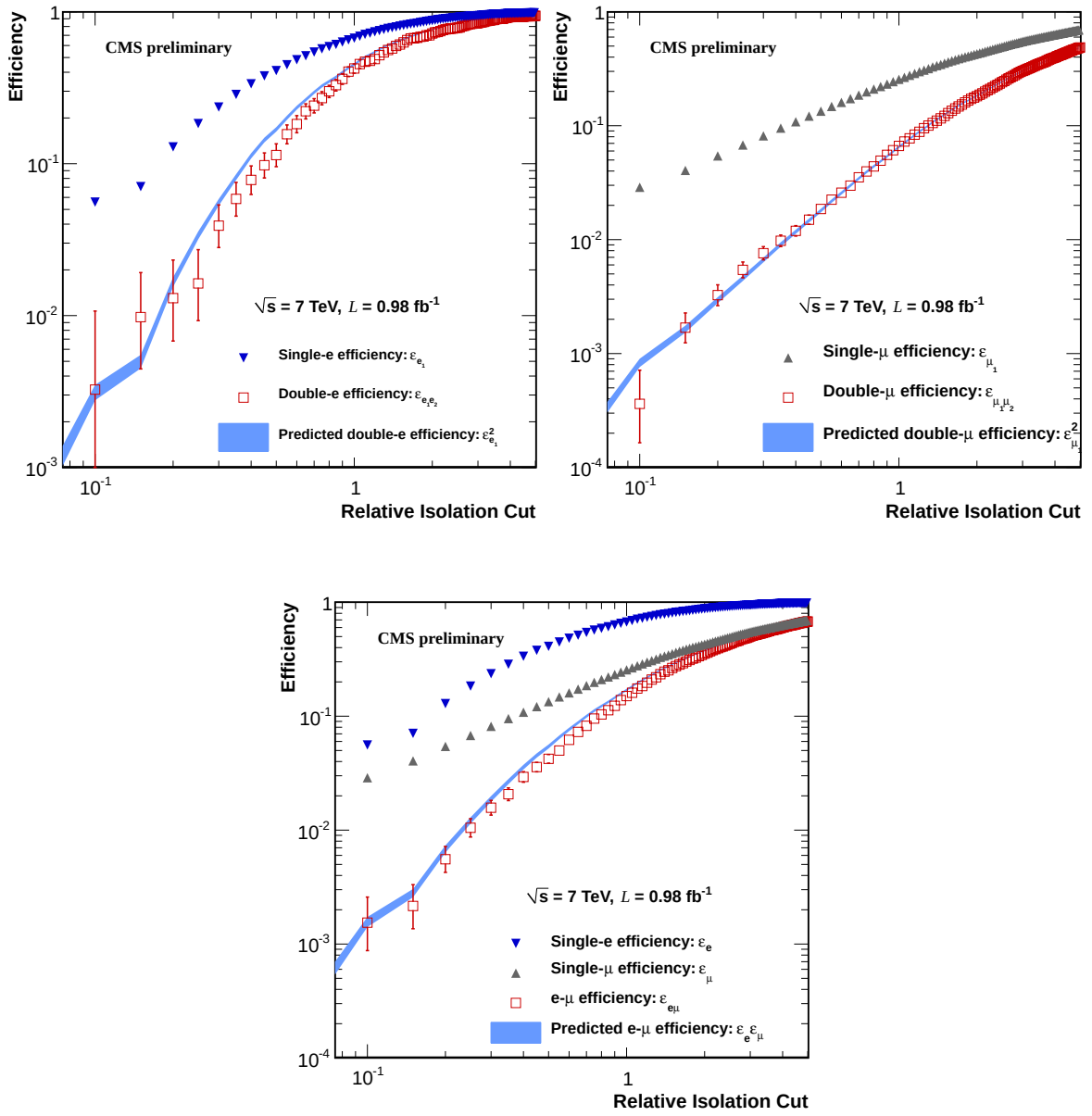

Figure 11: Efficiency of the isolation requirement as a function of the cut value in dielectron (top left), dimuon (top right), and electron-muon events (bottom). Single lepton efficiency is shown together with the observed distribution of the isolation requirement on both leptons compared to the product of single lepton efficiencies giving the predicted value.

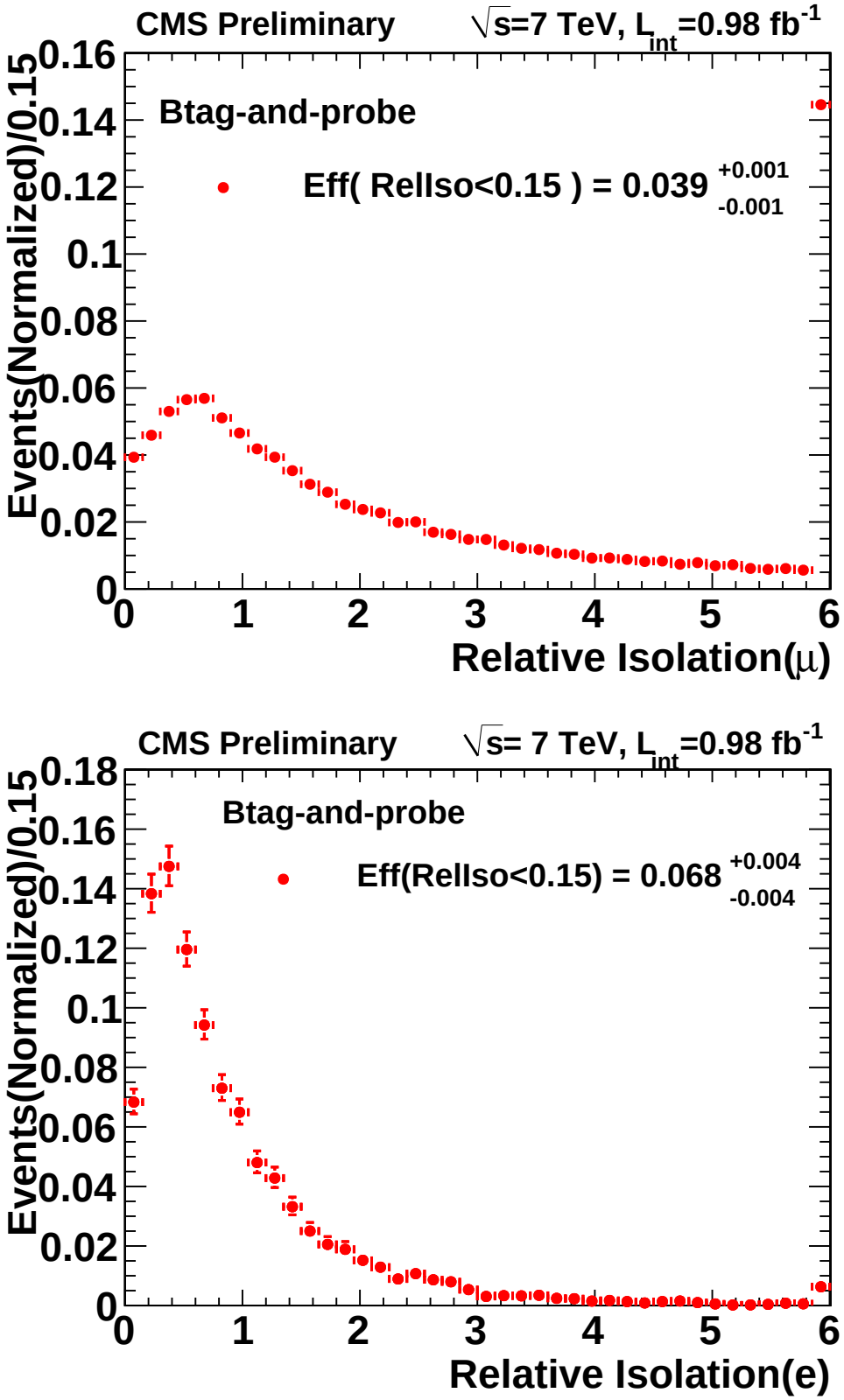

Figure 12: Isolation templates for muons (top) and electrons (bottom) used for the prediction of single-fake lepton backgrounds in Method (B).

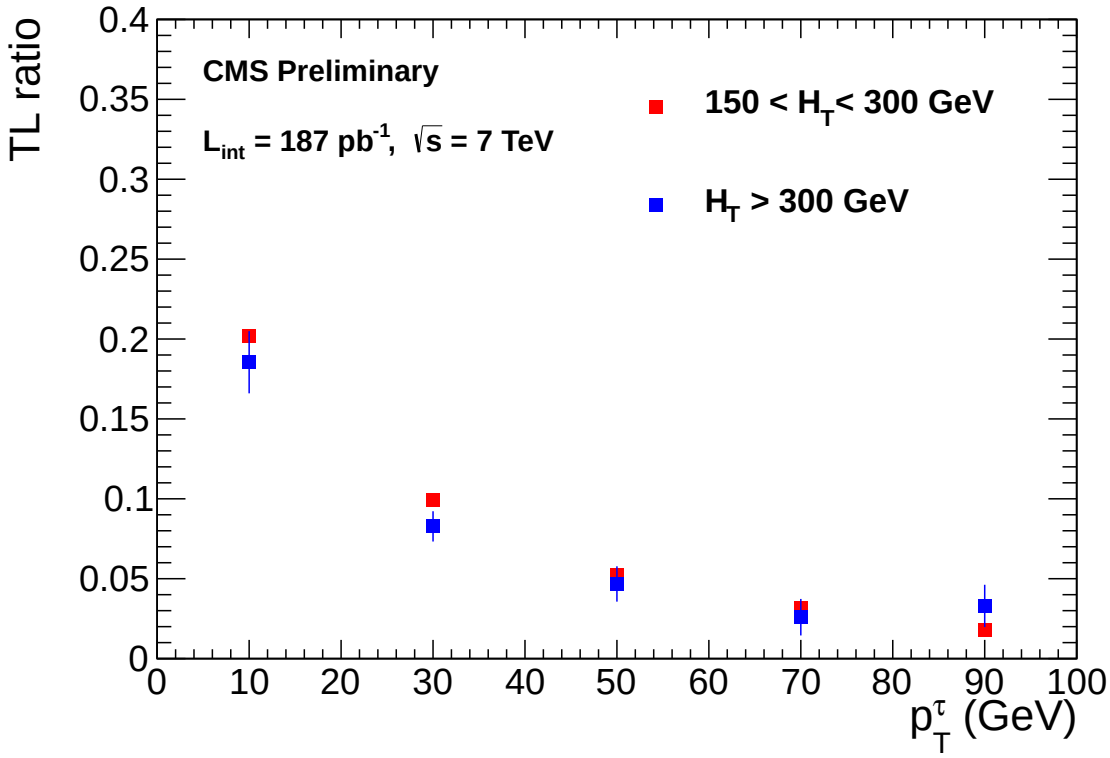

Figure 13: Tau TL ratio projected on p_T.

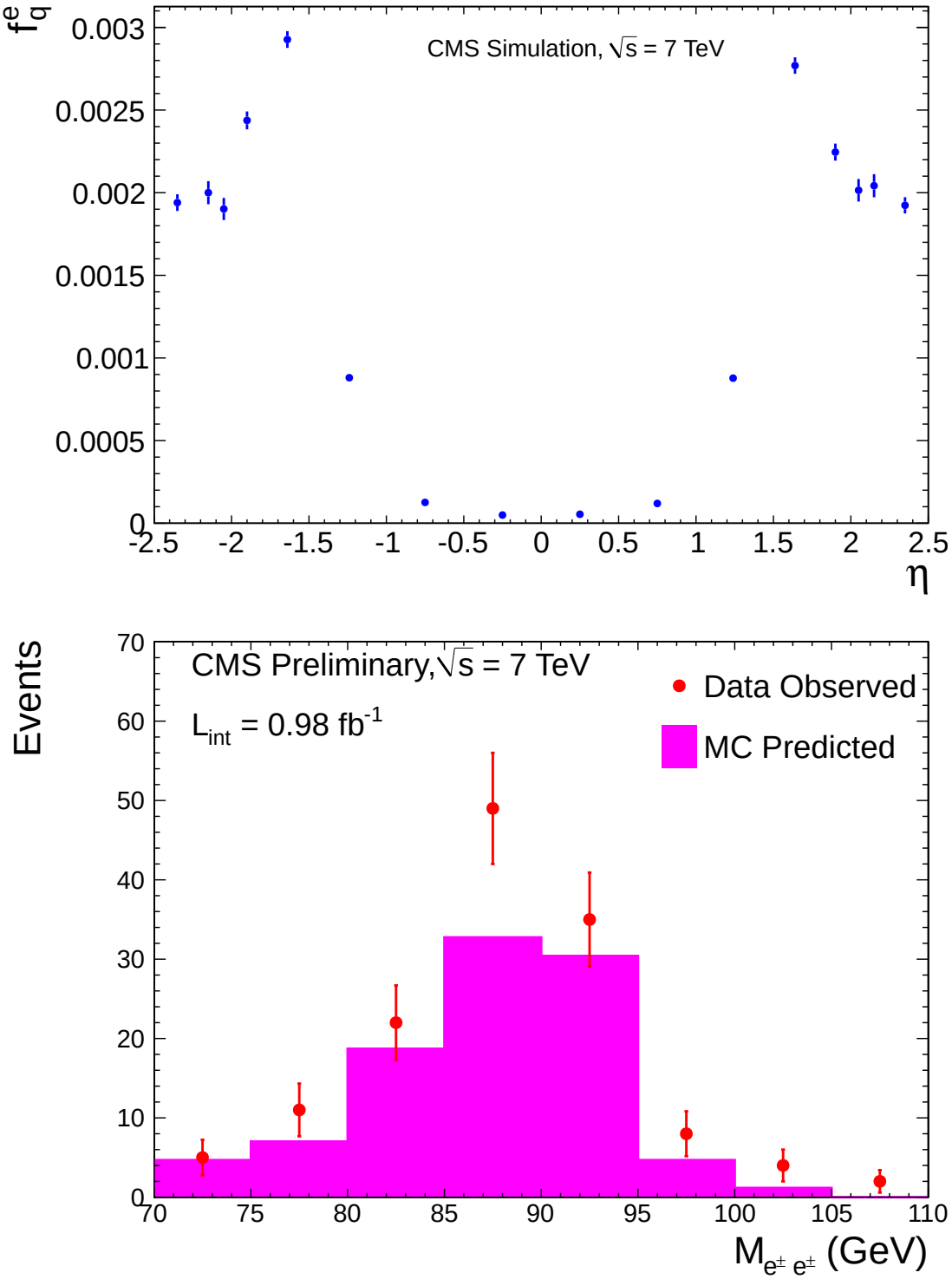

Figure 14: Charge misreconstruction probability for electrons projected on η, measured in simulated events (top). Same-sign dielectron invariant mass distribution in the Z-boson control region for data compared to that in simulation (bottom).

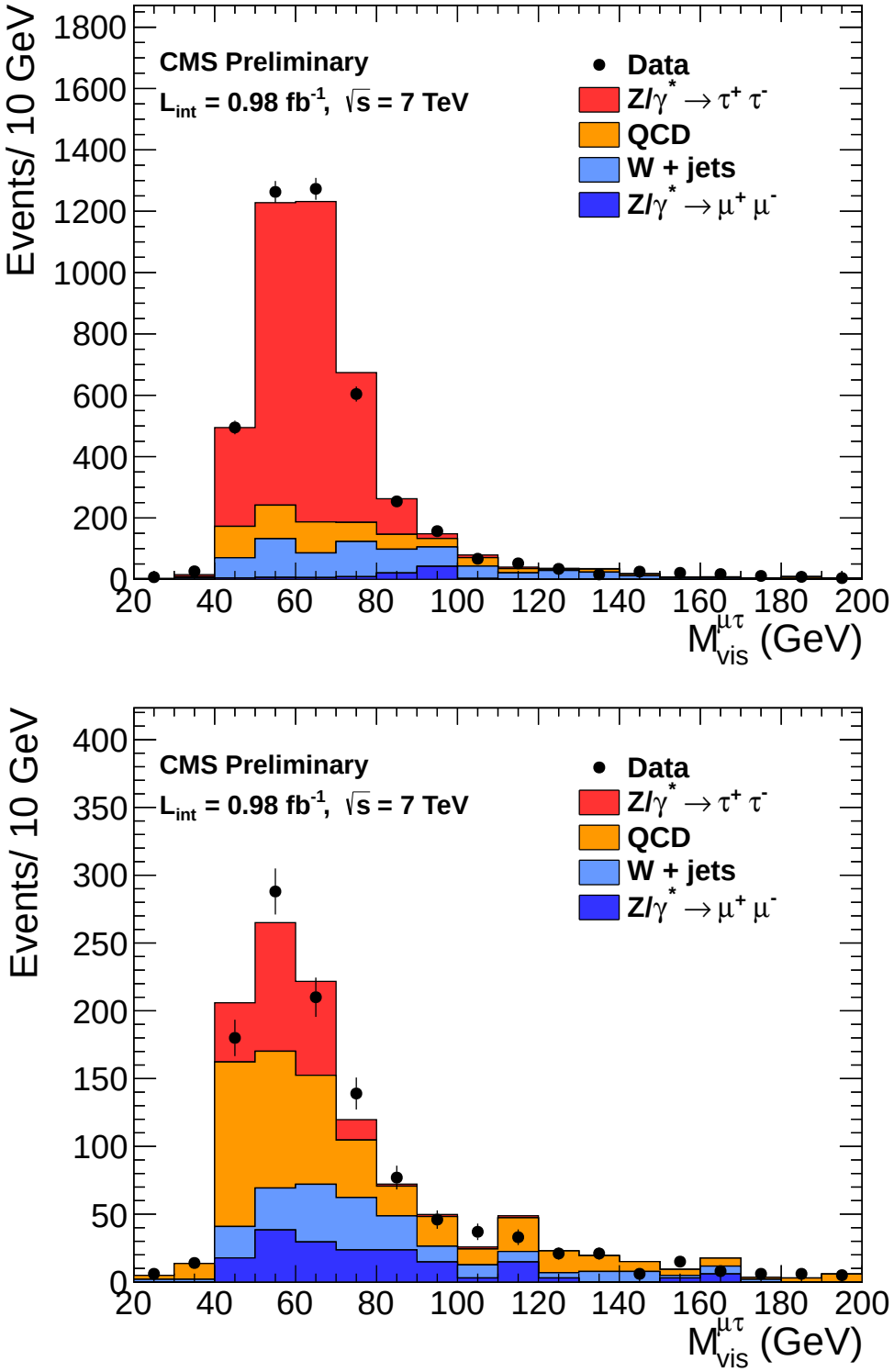

Figure 15: Distributions of the invariant mass of muon-tau pairs with opposite sign (top) and same sign (bottom). The invariant mass is computed using the tau visible momentum (does not include undetected neutrinos). The distributions compare contributions from events in data (points with error bars) and the expected signal and background contributions (filled histograms) with shapes taken from simulation and their relative contributions determined by a fit to the data points.

Table 7: A summary of the expected simulated background events and events with charge misreconstruction. The contributions to the simulated backgrounds are displayed separately by process: WZ/ZZ, $t\bar{t}W$, same-sign W-boson production in double-parton-pair scattering ($2 \times (q\bar{q} \to W^{\pm})$), double "W-strahlung" with same-sign W bosons ($qq \to q'q'W^{\pm}W^{\pm}$), and W/Z production in association with a photon ($V\gamma$).

Search Region (min. H_T / E_T^{miss})	WZ/ZZ	$t\bar{t}W$	$2 \times (q\bar{q} \to W^{\pm})$	$qq \to q'q'W^{\pm}W^{\pm}$	$V\gamma$	Charge misrec.	Total
Region 1 (400/120)							
Inclusive dileptons	0.06 ± 0.03	0.28 ± 0.01	0.00 ± 0.002	0.32 ± 0.02	0.00 ± 0.21	0.03 ± 0.01	0.7 ± 0.2
High–p_T dileptons	0.06 ± 0.03	0.26 ± 0.01	0.00 ± 0.002	0.31 ± 0.02	0.00 ± 0.21	0.03 ± 0.01	0.7 ± 0.2
τ dileptons	0.00 ± 0.01	0.04 ± 0.02	0.00 ± 0.002	0.05 ± 0.01	0.15 ± 0.15	0.8 ± 0.4	1.0 ± 0.4
Region 2 (400/50)							
Inclusive dileptons	0.10 ± 0.03	0.62 ± 0.02	0.002 ± 0.002	0.65 ± 0.03	0.00 ± 0.21	0.09 ± 0.02	1.5 ± 0.2
High–p_T dileptons	0.10 ± 0.03	0.59 ± 0.02	0.002 ± 0.002	0.63 ± 0.03	0.00 ± 0.21	0.09 ± 0.02	1.4 ± 0.2
Region 3 (200/120)							
Inclusive dileptons	0.20 ± 0.05	0.86 ± 0.02	0.002 ± 0.002	0.62 ± 0.02	0.00 ± 0.21	0.08 ± 0.01	1.8 ± 0.2
High–p_T dileptons	0.20 ± 0.05	0.79 ± 0.02	0.00 ± 0.002	0.57 ± 0.02	0.00 ± 0.21	0.08 ± 0.01	1.6 ± 0.2
Region 4 (80/100)							
High–p_T dileptons	0.43 ± 0.07	1.51 ± 0.02	0.004 ± 0.003	0.93 ± 0.03	0.00 ± 0.21	0.28 ± 0.03	3.2 ± 0.2

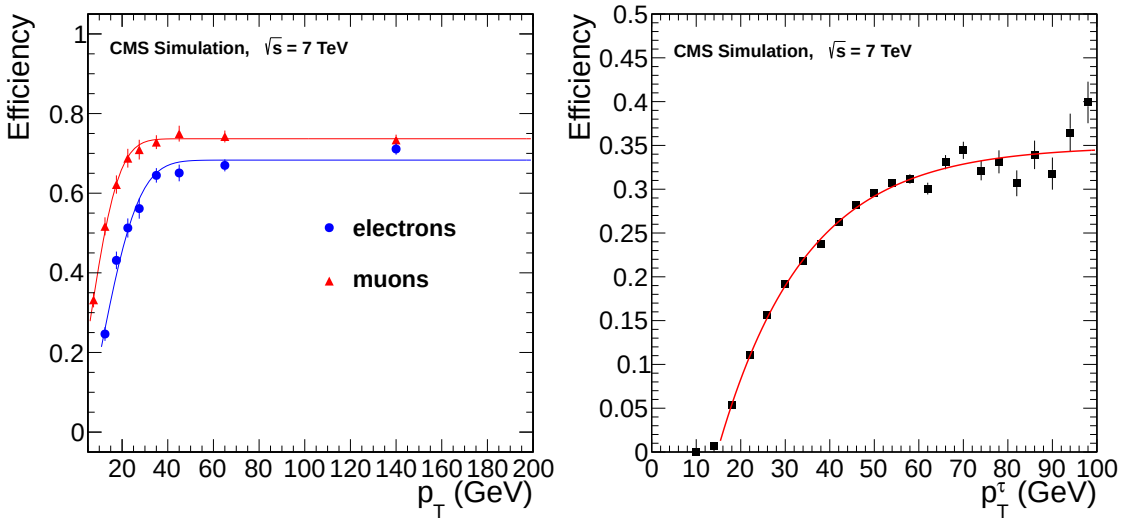

Figure 16: Electron and muon selection efficiency as a function of p_{T}, estimated in simulation LM6 benchmark point and corrected for simulation-to-data scale factors.

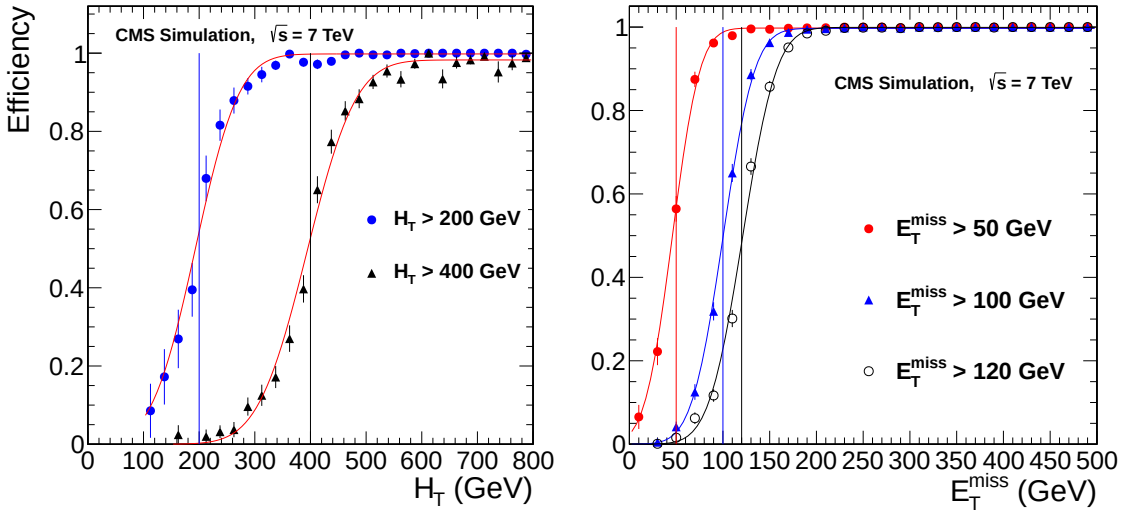

Figure 17: Efficiency for an event to pass a given reconstructed $E_{\mathrm{T}}^{\mathrm{miss}}$ (H_{T}) threshold as a function of generator level $E_{\mathrm{T}}^{\mathrm{miss}}$ (H_{T}). The curves are shown for $E_{\mathrm{T}}^{\mathrm{miss}}$ thresholds of 50, 100, 120 GeV; the thresholds for H_{T} are 200, and 400 GeV.

Table 8: Comparison of observed 95% CL upper limits computed with different statistical methods. Results are displayed for a limit set using Bayesian, and hybrid frequentist-Bayesian CL_s method [29]. For the CL_s technique, two results are reported: one obtained using the ratio of the signal-with-background and background-only likelihoods with central values of the nuisance parameters (LEP CL_s) and the other obtained with parameters, including the signal strength, maximizing the ratio (LHC CL_s). The main values for upper limits in this analysis are reported using the LHC CL_s method. Log-normal distributions for the nuisance parameters and a uniform signal strength are used in all methods.

Method	Bayesian	LEP CL_s	LHC CL_s
Inclusive dileptons			
Search region 1	4.0	3.8	3.7
Search region 2	9.2	9.1	8.9
Search region 3	7.5	7.5	7.3
High-p_{T} dileptons			
Search region 1	3.1	3.1	3.0
Search region 2	8.1	7.9	7.5
Search region 3	5.3	5.2	5.2
Search region 4	7.4	7.6	6.0
τ dileptons			
Search region 1	6.2	6.1	5.8